AgriVoltaics World Conference 2023

PV System Technologies

https://doi.org/10.52825/agripv.v2i.997

Published: 23 May 2024

Improved Land Use Efficiency Through Spectral Beam Splitting in Agrivoltaic Farms

Eshwar Ravishankar[1][https://orcid.org/0000-0001-8684-4113], Shir Esh[2,3,4], Offer Rozenstein[2], Helena Vitoshkin[3][https://orcid.org/0000-0003-2191-0049], Abraham Kribus[4], Gur Mittelman[4,5], Sanjeev Jakhar[6], and Ricardo Hernandez[1]

[1] Department of Horticultural Science, North Carolina State University, USA

[2] Institute of soil, water and environmental sciences, ARO – Volcani Institute, Israel

[3] Institute of Agricultural Engineering, ARO-Volcani Institute, Israel

[4] School of Mechanical Engineering, Faculty of Engineering, Tel Aviv University, Israel

[5] Afeka Tel-Aviv College of Engineering, Israel

[6] School of Mechanical Engineering, Vellore Institute of Technology, Chennai

Abstract. Installing photovoltaic (PV) collectors above arable land (Agrivoltaics) can aid with the shortage of available land area for solar power generation and food production. Most open field agrivoltaics are based on opaque PV devices which absorb photosynthetically active radiation (PAR, 400-700 nm), reducing crop yield and increasing variability in light distribution across the field. This research evaluates the performance of spectral beam splitter integrated photovoltaic (BSIPV) modules using a PV performance model. A high percentage (66 %) of PAR incident on the spectral beam splitter is transmitted effectively to the plants, while the near infrared radiation (NIR, > 700 nm) is reflected to the adjacent bifacial opaque photovoltaic module to generate power. In the model, seven rows of modules were placed uniformly across the field at a height of four meters from the ground. Considering a cool season (November – March) in Yuma, Arizona, in a conventional opaque PV agrivoltaic farm received 43 % lower total daylight integral (TDLI) across the season in comparison to open field with a coefficient of variation (ratio of standard deviation to mean expressed in percentage) of 56 % in TDLI across the field. On the other hand, the BSIPV agrivoltaic farm limited the drop in TDLI to 7 % in comparison to open field and the coefficient of variation to 14 % across the field. Thus, BSIPV showed a 36 % improvement in TDLI relative to the conventional opaque PV agrivoltaic farm. The results of the current study justify further research on the proposed collector concept.

Keywords: Agrivoltaics, Spectral Beam-Splitting, Computational Model

1. Introduction

The simultaneous use of areas of land for both crop production and solar power generation is known as agrivoltaics [1]-[2]. Such systems collocate photovoltaic (PV) systems in agricultural fields for both food production and energy generation and was conceptualized as a solution to the increasing land competition between food and energy production [3]. Currently, most agrivoltaic farms are based on solar power collection from standard, flat plate silicon PV (Si-PV) devices [4]-[5]. However, such PV panels absorb all incident light leading to significant drop, variability and delay in crop yield [6]-[7]. In addition to the drop in yield, the variable shading patterns under Si-PVs also cause low spatial uniformity in crop growth. The efficiency of the agrivoltaic system in comparison to a crop field and/or PV farm is described through land equivalent ratio (LER). LER gives the relative area required to produce the same amount of

crop yield and electricity in an agrivoltaic PV (APV) farm with respect to separated productions on different land surfaces [8]. Out of a theoretical maximum value of 2, the APV farms with Si-PV solar panels with and without solar tracking range between 1.2-1.7 for different crops [3], [9]–[11].

A proposed strategy to increase LER is to increase plant yield and reduce variability in yield. A plausible solution, proposed in this research, is to allow sunlight required for photosynthesis to reach the plants while also using other portions of the sunlight for power generation through the use of a wavelength selective spectral beam splitter mirrors (SBSM). Such SBSM systems have previously been used for cogeneration where incident sunlight is spectrally distributed and captured efficiently for solar heat collection and power generation through thermal receiver and PV module [12]. However, such SBSM systems till date have not been utilized to share sunlight between crop production and energy harvesting in agrivoltaic farms. A pair of SBSM system is placed at a 45° to the adjacent BPV. The collector involves only planar, solid-state elements and 1-axis tracking. When appropriately oriented, a major fraction of incident sunlight within ePAR wavelength region is transmitted for plant growth. At the same time, sunlight within the near infrared (NIR, > 750 nm) wavelength region is almost completely reflected to the BPV for power generation [12]. Therefore, the use of wavelength selective spectral beam splitter mirrors (SBSM) in tandem with bifacial PVs (BPV) is expected to improve LER and crop growth through the significant transmittance of radiation required for photosynthesis [12]. While the concept holds promise, there is a need to develop a modeling framework that quanitifies the differences in light intensities under the SBSM-BPV panels in comparison to conventional Si-PV system in an agrivoltaic farm by considering row and column spacing, PV and SBSM system dimensions, weather conditions, etc. This modeling framework is highlighted in this work.

2. Methods

To understand the concept of SBSM-BPV AV farm, we model a field length and width of 50 x 50 m^2. The BPV system has dimensions of 1.02 x 1.04 m^2 with the corresponding SBSM system having dimension of 1.50 x 1.02 m^2. The pitch (row-to-row separation) between them is 6 m. Spacing within each row is 4 m. This results in 12 rows and 8 columns of SBSM-BPV systems respectively across the complete AV farm. For the bifacial PV, the surface facing the sky is taken as front surface whereas the other surface is considered as back surface of the module. The daily integration method was used to determine the beam (direct), diffuse and ground reflected radiation incident on the agrivoltaic system [13]. Effective incident angles for diffuse and reflected solar radiation incident on the surface of the agrivoltaic system were computed assuming isotropic light scattering conditions. Inputs of this model include the terrestrial monthly average, daily total, and diffuse radiation on a horizontal surface, which was obtained for each location from NSRDB [14].The function of the system is depicted using Yuma, Arizona as the weather conditions for operation.

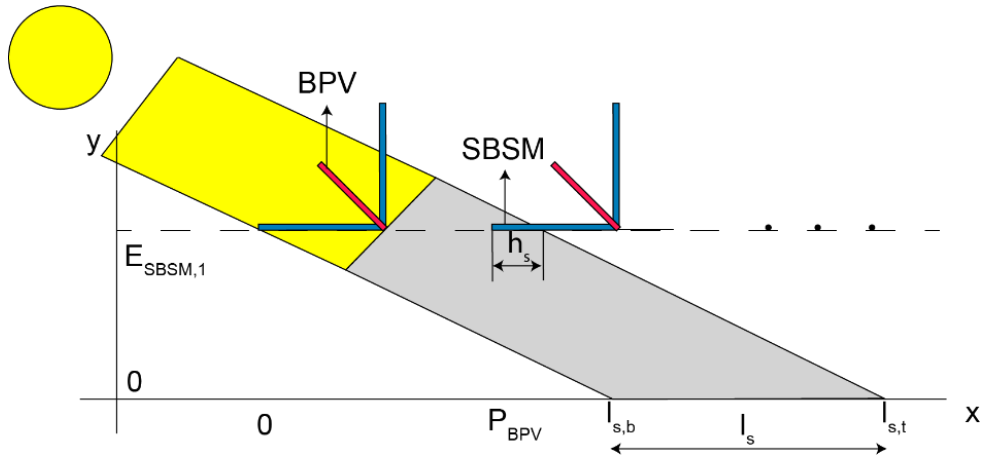

Figure 1. Illustration of direct sunlight incident on SBSM system and the corresponding shadow on the ground.

2.1 Calculating light distribution in the field under SBSM-BPV system

To compute the contribution of solar irradiation on the SBSM system, the AOI is defined as 45°. Accordingly, the tilt angle and azimuth of the complete SBSM-BPV system are adjusted through a dual axis tracking system by defining the starting elevation and starting azimuth. This is given by [13]:

$$\mathrm{A} = (\mathrm{N}.\sin(\mathrm{al}_{\mathrm{final}})) + (\mathrm{C}.\cos(\mathrm{al}_{\mathrm{final}})).\cos(\mathrm{U}) \quad (2.1)$$

where, al_{final} is the calculated solar panel altitude obtained from tracking sun (°).

$$(\mathrm{C}.\sin(\mathrm{U})) = (\mathrm{N}.\mathrm{D}.\sin(\mathrm{al}_{\mathrm{final}})) - (\mathrm{C}.\mathrm{D}.\sin(\mathrm{al}_{\mathrm{final}})).\cos(\mathrm{U}) \quad (2.2)$$

where, $\mathrm{C} = \cos(\mathrm{SE})$ (2.3)

where, SE is the starting elevation angle of SBSM system (°)

$$\mathrm{N} = \sin(\mathrm{SE}) \quad (2.4)$$

$$\mathrm{A} = \cos(\mathrm{AOI}_{\mathrm{dir}}) \quad (2.5)$$

where, AOI_{dir} is the angle of incidence of direct solar radiation on SBSM system (°)

$$\mathrm{U} = \mathrm{SA} - \mathrm{az}_{\mathrm{final}} \quad (2.6)$$

where, az_{final} is the calculated solar panel altitude obtained from tracking sun (°).

$$\mathrm{P} = (\mathrm{C}.\cos(\mathrm{az}_{\mathrm{final}}).\sin(\mathrm{SA})) - (\mathrm{C}.\cos(\mathrm{SA}).\sin(\mathrm{az}_{\mathrm{final}})) \quad (2.7)$$

where, SA is the starting angle (°)

$$\mathrm{Q} = (\mathrm{N}.\cos(\mathrm{al}_{\mathrm{final}})) - (\sin(\mathrm{al}_{\mathrm{final}}).\mathrm{C}.\cos(\mathrm{U})) \quad (2.8)$$

$$\mathrm{D} = \frac{\mathrm{P}}{\mathrm{Q}} \quad (2.9)$$

The gap between the BPV system across rows is given by

$$\mathrm{D}_{\mathrm{BPV}} = \mathrm{P}_{\mathrm{BPV}} - (\mathrm{W}_{\mathrm{BPV}}.\cos(\mathrm{TA}_{\mathrm{BPV}})) \quad (2.10)$$

where, P_{BPV} are the gap between the BPV system between rows (m), L_{BPV} and W_{BPV} are the horizontal length and width of the BPV system respectively (m).

The number of rows and columns of BPV in an agrivoltaic farm are given by

$$\mathrm{Nr1}_{\mathrm{SBSM-BPV}} = \frac{(\mathrm{W}_{\mathrm{AV}}/\mathrm{L}_{\mathrm{BPV}})}{\mathrm{AR}_{\mathrm{AV}}.\left(\cos(\mathrm{TA}_{\mathrm{BPV}})+\left(\frac{\mathrm{D}_{\mathrm{BPV}}}{\mathrm{L}_{\mathrm{BPV}}}\right)\right)} \quad (2.11)$$

where, AR_{AV} is the aspect ratio of the agrivoltaic farm which is the ratio of width to length of the field, W_{AV} and L_{AV} is the width and length of the agrivoltaic farm respectively (m).

$$\mathrm{E}_{\mathrm{SBSM,2}} = \mathrm{E}_{\mathrm{SBSM,1}} + (\mathrm{L}_{\mathrm{SBSM}}.\sin(\mathrm{TA}_{\mathrm{SBSM}})) \quad (2.12)$$

where, $E_{SBSM,1}$ is the smaller of the two heights of the SBSM system (m), $E_{SBSM,2}$ is the larger of the two heights of the SBSM system (m), TA_{SBSM} is tilt angle of the SBSM system (°).

The shadow lengths cast by the direct beam of the sun on ground along the pitch or on the adjacent SBSM system is depicted in Figure 1. For any given angle of incidence, the lengths of the shadow cast by the top and bottom points of the SBSM on the ground measured from x=0 is denoted by $l_{s|t}$ and $l_{s|back}$ respectively (m) and given by

$$l_{s|t} = \frac{(E_{SBSM,1}+L_{SBSM}.\sin(TA_{SBSM})).\cos(AOI_{dir})}{\sin(90-TA_{SBSM}+AOI_{dir}).\sin(TA_{SBSM})} \quad (2.13)$$

$$l_{s|back} = \frac{E_{SBSM,1}-\cos(AOI_{dir})}{\sin(90-TA_{SBSM}+AOI_{dir}).\sin(TA_{SBSM})} \quad (2.14)$$

where, AOI_{dir} is angle of incidence of light with respect to the normal of SBSM system (°), L_{SBSM} is the length of SBSM system (m).

$$l_s = l_{s|t} - l_{s|back} \quad (2.15)$$

where, l_s is the actual shadow length on the ground (m)

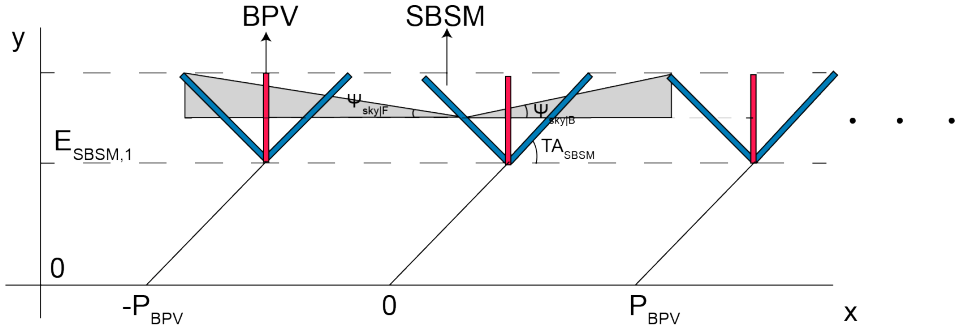

Figure 2. Masking of diffuse light on the face of the SBSM system by the adjacent systems on either side.

If $l_s > P_{BPV}$ then a part of the shadow will be cast on the adjacent system with shadow height denoted by h_s (m) and is given by [15-16]

$$h_s = \frac{\sin(90+AOI_{dir}-TA_{SBSM}).(l_{s|t}-P_{BPV})}{\sin(90-AOI_{dir})} - \frac{E_{SBSM,1}}{\sin(TA_{SBSM})} \quad (2.16)$$

The direct solar irradiation on the unshaded part of the front module surface (i.e. $h>h_s$) after accounting for surface reflection is given by,

$$S_{SBSM,dir}(z) = \begin{Bmatrix} \int_0^{L_{SBSM}} \frac{(1-\delta(AOI_{dir})).S_{dir,i}.\cos(AOI_{dir})}{P_{BPV}} z > h_s \\ 0. z < h_s \end{Bmatrix} \quad (2.17)$$

where, $S_{SBSM,dir}$ is the direct solar irradiation after accounting for surface reflection (W/m2) Sdir,i is the direct solar irradiance (W/m2). Similarly, irradiance on the back panel is also calculated. Irradiance is also calculated for SBSM systems within the same row.

For diffuse radiation we first determine the masking of diffuse light on the SBSM system by the adjacent modules. Let's consider a point z along the height of the SBSM, the masking angles of diffuse light for front and back surfaces are denoted by Ψsky|F and Ψsky|B as shown in Figure 2.

$$\Psi_{sky|F}(z) = \tan^{-1}\left(\frac{L_{SBSM}-z.\sin(TA_{SBSM})}{P_{BPV}-(L_{SBSM}-z).\cos(TA_{SBSM})}\right) \quad (2.18)$$

$$S_{SBSM,dif|F}(z) = S_{dif,i}.F_{dz\rightarrow sky|F} \quad (2.19)$$

where, $S_{dif,i}$ is the incident diffuse radiation (W/m^2), $S_{SBSM,dif|F}$ is the incident diffuse radiation on the front facing surface of SBSM w.r.t. sky (W/m^2).

$$F_{dz\rightarrow sky|F}(z) = 0.5.\left(1 - \sin\left(\Psi_{sky|F}(z)\right)\right) \quad (2.20)$$

where, $F_{dz\rightarrow sky|F}$ is the view factor of the front of SBSM system w.r.t. sky,

$$\Psi_{sky|B}(z) = \tan^{-1}\left(\frac{L_{SBSM} - z.\sin(TA_{SBSM})}{P_{BPV} + (L_{SBSM} - z).\cos(TA_{SBSM})}\right) \quad (2.21)$$

$$S_{SBSM,dif|B}(z) = S_{dif,i}.F_{dz\rightarrow sky|B} \quad (2.22)$$

where, $S_{SBSM,dif|B}$ is the incident diffuse radiation on the back facing surface of SBSM w.r.t. sky (W/m^2).

$$F_{dz\rightarrow sky|B}(z) = 0.5.\left(1 - \sin\left(\Psi_{sky|B}(z)\right)\right) \quad (2.23)$$

where, $F_{dz\rightarrow sky|B}$ is the view factor of the front of SBSM system w.r.t. sky,

$$S_{SBSM,dif} = \frac{1}{P_{BPV}}.\int_0^{L_{SBSM}} \left(S_{SBSM,dif|F}(z) + S_{SBSM,dif|B}(z)\right) dz \quad (2.24)$$

where, $S_{SBSM,dif}$ is the total diffuse solar irradiation on the SBSM system (W/m^2). The direct and diffuse reflected radiation are computed in a manner similar to diffuse radiation.

A two-dimensional model for spatial shade distribution is developed to better understand the edge effects due to direct light obstruction from SBSM system. To calculate the amount of direct light shadowing at any observation point (OP) due to the SBSM system, we assimilate the SBSM systems as polygons with four edges defined through their cartesian coordinates (x_e, y_e, z_e). The coordinates of observation points (x_{op}, y_{op}, z_{op}) as well as for the SBSM were calculated with reference to an arbitrary point of origin located at north-east corner of the field. The solar coordinates for a given OP with respect to a SBSM are then calculated in terms of elevation ($el_{op->s}$) and azimuth ($az_{op->s}$) angles using [15]

$$el_{op\rightarrow s} = \sin^{-1}\left(\frac{z_e - z_{op}}{\sqrt{(x_e - x_{op})^2 + (y_e - y_{op})^2 + (z_e - z_{op})^2}}\right) \quad (2.25)$$

$$az_{op\rightarrow s} = \cos^{-1}\left(\frac{y_e - y_{op}}{\sqrt{(x_e - x_{op})^2 + (y_e - y_{op})^2}}\right) \quad (2.26)$$

$el_{op\rightarrow s}$, $az_{op\rightarrow s}$ for all SBSM systems in the field were calculated and were compared with corresponding angles for the sun. This was used to find whether there is any obstruction to the direct path from the sun to the OP due to the SBSM-BPV system.

3. Results and Discussion

Sunlight in the ePAR spectra (400-750 nm) directly influences crop rate of photosynthesis and hence its yield. The SBSM system has a transmittance of 65 percent over the ePAR spectra. The average availability of light in the ePAR spectra only reduces by 2 percent across the entire AV farm in Yuma, AZ. In comparison to the open field, the variability in ePAR light is

increased by 6 percent across the entire year. A reason for the significantly lower reduction in ePAR radiation in comparison to the transmittance of the SBSM-BPV system is attributed the spacing between various systems across the AV farm. We see that the area of AV farm shaded by the SBSM-BPV systems is only 20 percent of the total available area. The remaining area of the AV farm receives light comparable to that of an open field. A schematic of the direct ePAR light distribution across the AV farm for the complete growth season in Yuma AZ is shown in Figure 3(A). In the region of the field where solar radiation is obstructed by the SBSM-BPV system, the average DLI across the entire harvest cycle reduces by a maximum of 40 percent. Considering a 4 m2 region of the field around the SBSM-BPV system (highlighted by color gradients other than red in Figure 3(A)) the average reduction in DLI is only around 20 percent while the increase in light variability is around 17 percent.

In the region of the field where solar radiation is obstructed by Si-PV system (Figure 3(B)), we see that almost the complete direct ePAR radiation is obstructed. Considering a 4 m2 region of the field around the SBSM-BPV system the average reduction in DLI is 33 percent while the increase in light variability is around 48 percent. This is almost three times the variability and 13 percent lower light availability at crop level in comparison to the SBSM-BPV system. Over the course of that entire day, this fractional area of shading remains consistent due to the presence of dual-axis tracking capability for the SBSM-BPV system. This ensures that the angle of incidence of sunlight on the SBSM system is nearly the same across climates year-around.

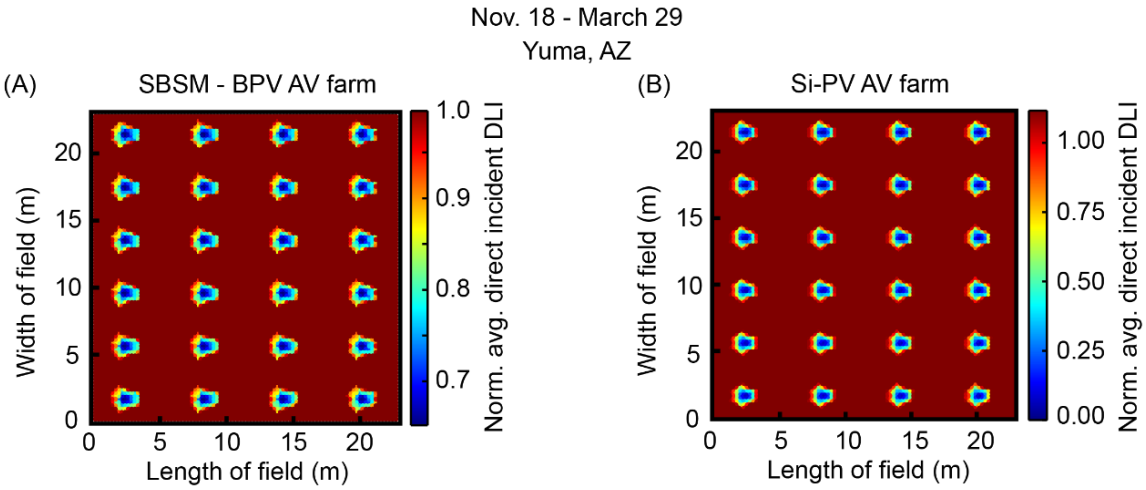

Figure 3. Schematic of SBSM-BPV AV farm in Yuma, AZ depicting (C) direct ePAR light distribution, (D) Total direct light above crop level

4. Conclusion

Currently, most agrivoltaic farms are based on solar power collection from standard, flat plate Si-PV devices. These systems provide high efficiency but also absorb all incident light leading to drop in crop yield. Hence, the design and implementation of SBSM systems in tandem with BPV to further improve land use efficiency and crop growth through the transmittance of a larger fraction of ePAR radiation. Here, we formulated a model to gain an improved understanding of the potential of SBSM-BPV system towards deployment in agrivoltaic farms in terms of variability in light conditions. Here, the location considered is Yuma. Through the modeling process, we show that More improvements are expected to be achieved with the optimization of the splitter optical properties and PV modules material, as well as row spacing

and collectors tracking algorithm. The result from this model provides a clear view of the opportunity to achieve more sustainable agricultural practices.

Author contributions

Ricardo Hernandez directed the study. Eshwar Ravishankar formulated the model with contributions from Abraham Kribus, Helena Vitoshkin, Offer Rozenstein, Gur Mittelman, Shir Esh, and Sanjeev Jakhar. Eshwar Ravishankar wrote the original draft and all authors contributed to the analysis and writing.

Competing interests

Competing interests arise when issues outside research may fairly be viewed as impacting the work's neutrality. All potential competing interests must be disclosed ("The authors declare the following competing interests: …"). If there are no potential competing interests please state "The authors declare no competing interests."

Funding

The authors would like to acknowledge the Ministry of Energy of Israel (grant no. 219-11-125) and the US-Israel binational agricultural research and development fund (BARD) (US-5236-20).

Acknowledgement

The authors would like to acknowledge the computing resources provided by North Carolina State University High Performance Computing Service Core Facility (RRID:SCR 022168).

References

1. S. Nonhebel, "Renewable energy and food supply: Will there be enough land?," *Renew. Sustain. Energy Rev.*, vol. 9, no. 2, pp. 191–201, 2005, doi: 10.1016/j.rser.2004.02.003.

2. Goetzberger and A. Zastrow, "On the Coexistence of Solar-Energy Conversion and Plant Cultivation," *Int. J. Sol. Energy*, vol. 1, no. 1, pp. 55–69, 1982, doi: 10.1080/01425918208909875.

3. H. Dinesh and J. M. Pearce, "The potential of agrivoltaic systems," *Renew. Sustain. Energy Rev.*, vol. 54, pp. 299–308, 2016, doi: 10.1016/j.rser.2015.10.024.

4. S. Gorjian *et al.*, "Progress and challenges of crop production and electricity generation in agrivoltaic systems using semi-transparent photovoltaic technology," *Renew. Sustain. Energy Rev.*, vol. 158, no. January, pp. 112126–112149, 2022, doi: 10.1016/j.rser.2022.112126.

5. M. A. Al Mamun, P. Dargusch, D. Wadley, N. A. Zulkarnain, and A. A. Aziz, "A review of research on agrivoltaic systems," *Renew. Sustain. Energy Rev.*, vol. 161, no. March, pp. 112351–112367, 2022, doi: 10.1016/j.rser.2022.112351.

6. J. A. Hollingsworth, E. Ravishankar, B. O'Connor, J. X. Johnson, and J. F. DeCarolis, "Environmental and economic impacts of solar-powered integrated greenhouses," *J. Ind. Ecol.*, vol. 24, no. 1, pp. 234–247, 2020, doi: 10.1111/jiec.12934.

7. M. Cossu *et al.*, “Solar radiation distribution inside a greenhouse with south-oriented photovoltaic roofs and effects on crop productivity,” *Appl. Energy*, vol. 133, pp. 89–100, 2014, doi: 10.1016/j.apenergy.2014.07.070.

8. N. C. Giri and R. C. Mohanty, “Agrivoltaic system: Experimental analysis for enhancing land productivity and revenue of farmers,” *Energy Sustain. Dev.*, vol. 70, pp. 54–61, 2022, doi: 10.1016/j.esd.2022.07.003.

9. C. Dupraz, H. Marrou, G. Talbot, L. Dufour, A. Nogier, and Y. Ferard, “Combining solar photovoltaic panels and food crops for optimising land use: Towards new agrivoltaic schemes,” *Renew. Energy*, vol. 36, no. 10, pp. 2725–2732, 2011, doi: 10.1016/j.renene.2011.03.005.

10. B. Valle *et al.*, “Increasing the total productivity of a land by combining mobile photovoltaic panels and food crops,” *Appl. Energy*, vol. 206, no. September, pp. 1495–1507, 2017, doi: 10.1016/j.apenergy.2017.09.113.

11. H. A. Al-Agele, K. Proctor, G. Murthy, and C. Higgins, “A case study of tomato (Solanum lycopersicon var. legend) production and water productivity in agrivoltaic systems,” *Sustain.*, vol. 13, no. 5, pp. 1–13, 2021, doi: 10.3390/su13052850.

12. G. Mittelman and A. Kribus, “Innovative Solar Spectral Beam Splitting Concepts: Alternative Fuels Production,” *35th Eur. Photovolt. Sol. Energy Conf. Exhib.*, vol. 6, no. 11, pp. 1895–1898, 2018.

13. DY Goswami. Principles of Solar Engineering. 3rd ed. Boca Raton: CRC Press, 2015.

14. M. Sengupta, Y. Xie, A. Lopez, A. Habte, G. Maclaurin, J. Shelby. The National Solar Radiation Data Base (NSRDB). Renewable and Sustainable Energy Reviews vol. 89, pp. 51–60, 2018, doi: 10.1016/j.rser.2018.03.003.

15. P. E. Campana, B. Stridh, S. Amaducci, and M. Colauzzi, “Optimisation of vertically mounted agrivoltaic systems,” *J. Clean. Prod.*, vol. 325, no. July, p. 129091, 2021, doi: 10.1016/j.jclepro.2021.129091.

16. M. H. Riaz, R. Younas, H. Imran, M. A. Alam, and N. Z. Butt, “Module Technology for Agrivoltaics: Vertical Bifacial vs. Tilted Monofacial Farms,” vol. 11, no. 2, pp. 1–29, 2019, [Online]. Available: http://arxiv.org/abs/1910.01076.